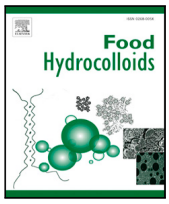
Food Hydrocolloids 176 (2026) 112567



Contents lists available at ScienceDirect

Food Hydrocolloids

journal homepage: www.elsevier.com/locate/foodhyd



From gels to high-moisture extrudates: pH and 11S:7S globulin ratio govern multiscale structure formation

Ekaterina D. Garina [a], Sam A. Kuijpers [b], Martijn I. Gobes [b], Gregory N. Smith [c], Michael Sztucki [d], Arno G.B. Wouters [e], John P.M. van Duynhoven [b,f,*], Wim G. Bouwman [a]

[a] Department of Radiation Science and Technology, Delft University of Technology, Mekelweg 15, 2629 JB Delft, The Netherlands
[b] Laboratory of Biophysics, Wageningen University and Research, Stippeneng 4, 6708WE Wageningen, The Netherlands
[c] ISIS Neutron and Muon Source, Science and Technology Facilities Council, Rutherford Appleton Laboratory, Chilton, Oxon OX11 0QX, UK
[d] ESRF, The European Synchrotron Radiation Facility, 71 Avenue des Martyrs, CS40220, 38043 Grenoble Cedex 9, France
[e] Laboratory of Food Chemistry and Biochemistry and Leuven Food Science and Nutrition Research Centre (LFoRCe), KU Leuven, Kasteelpark Arenberg 20, B-, 3001 Leuven, Belgium
[f] Unilever Global Foods Innovation Centre, Bronland 14, 6708 WH Wageningen, The Netherlands

ARTICLE INFO

Keywords:
Soy proteins
Protein composition
pH-effect
Structure formation
Small-angle scattering (SAS)

ABSTRACT

Soy protein isolates (SPIs) and concentrates (SPCs), which primarily consist of glycinin (11S globulin) and β-conglycinin (7S globulin), are the dominant ingredients in the production of plant-based meat products using high-moisture extrusion (HME). Yet the links between their gelation and structure formation under HME are not fully understood. In this work, we employ small-angle scattering (SAS) techniques, complemented by rheology, on heat-set gels to elucidate the multiscale aggregation pathways of fractionated 11S and 7S globulins, and relate these to the extrudate structure. Heat-set gels revealed a three-level structural hierarchy: compact protein units that persist after heating; aggregates whose mid-scale size and morphology vary with pH; and networks characterised by clustering strength. Near the isoelectric point (pI), both globulin-enriched fractions formed particulate gels. Under these conditions, 7S globulin-enriched gels were stiffer because their smaller aggregates created a higher density of contacts per unit volume, resulting in a higher clustering strength. Away from the pI, fibrillar aggregation dominated, and 11S globulin-enriched gels became stiffer as a result of forming thicker and more tightly connected strands. At pH 7, blending experiments revealed that even small additions of 7S globulin weaken the gels; however, under HME, the same additions enhance anisotropy. Specifically, 7S globulin promotes deformability and alignment, while 11S globulin contributes to network strengthening through covalent crosslinks. Together, these results establish parallels between heat-induced gelation and extrusion, highlighting the complementary roles of 11S and 7S globulins in structuring high-moisture extrudates of soy proteins.

1. Introduction

Due to their widespread availability and processing capabilities, soy protein isolates (SPIs) and concentrates (SPCs) are the most commonly used ingredients in the production of meat alternatives using high-moisture extrusion (HME). They comprise two major components, glycinin (belongs to the 11S globulin family) and β-conglycinin (belongs to the 7S globulin family), which account for about 31%–42% and 25%–37% of the total protein content, respectively (Verfaillie, Li, Janssen, et al., 2024). The soy 11S globulin is a hexamer with a molecular weight of about 300–380 kDa, composed of acidic (~35 kDa) and basic (~20 kDa) polypeptides linked by a disulphide bond (Badley et al., 1975; Staswick et al., 1984). The soy 7S globulin is a trimer with a molecular weight of about 150–200 kDa and is composed of α (~68 kDa), α' (~72 kDa), and β (~52 kDa) glycosylated subunits, which are linked by hydrophobic and electrostatic bonds (Thanh & Shibasaki, 1977).

The structural differences between the 11S and 7S globulins contribute to variations in their physical and functional properties, including aggregation and gelation, the most important functional attributes for meat alternative production. When heated beyond their denaturation temperatures at neutral pH, 11S globulin demonstrates a higher degree of aggregation compared to 7S globulin Guo et al. (2012),

* Corresponding author at: Laboratory of Biophysics, Wageningen University and Research, Stippeneng 4, 6708WE Wageningen, The Netherlands.
E-mail address: john.vanduynhoven@wur.nl (J.P.M. van Duynhoven).

https://doi.org/10.1016/j.foodhyd.2026.112567
Received 29 November 2025; Received in revised form 30 January 2026; Accepted 16 February 2026
Available online 17 February 2026
0268-005X/© 2026 The Authors. Published by Elsevier Ltd. This is an open access article under the CC BY license (http://creativecommons.org/licenses/by/4.0/).

attributed to its high content of hydrophobic amino acids in the basic polypeptides (Yuan et al., 2009). In contrast, the hydrophilic extension regions in α and α'-subunits of 7S globulin contribute to repulsive interactions that limit its aggregation. As a result, when blended, 7S soy globulin can terminate the growth of insoluble 11S aggregates (Damodaran & Kinsella, 1982; Guo et al., 2012). Furthermore, the low cysteine content in 7S globulin allows it to form thermally reversible gels, stabilised primarily by hydrogen bonding and hydrophobic interactions (Kinsella, 1979; Utsumi & Kinsella, 1985). In contrast, 11S globulin, being richer in cysteine (Kinsella, 1979), forms thermally irreversible gels that have a more rigid and elastic texture than 7S globulin gels (Yang et al., 2024).

The properties of protein gels are influenced not only by their composition but also by the conditions used to induce gelation. The physical integrity of these gels relies on the balance between the attractive and repulsive forces of the protein molecules in the system (Hermansson, 1979). At a pH near the isoelectric point (pI), proteins have a reduced electric charge and increased hydrophobic interactions, resulting in random aggregation and the formation of opaque, particulate-type gels. Conversely, when the pH shifts away from the pI, proteins exhibit an increased net charge and solubility, resulting in the transition from opaque to translucent, strand-type globular protein gels (Doi & Kitabatake, 1989).

In light of the above, differences in aggregation and gelation pathways are expected to translate into differences in structure development during HME. In our previous work (Kuijpers et al., 2025), we explored how pH-shifting via the water feed affects the multiscale structural anisotropy of HM extrudates of soy proteins. We showed that pH-shifting had a non-monotonic effect on texture and anisotropy across length scales: both hardness and structural anisotropy were minimal at pH $\sim$ pI and pH $\gg$ pI, with an optimum at pH > pI. Specifically, Magnetic Resonance Imaging (MRI) data showed that aligned lamellar phase-separated structures were absent at the pI, emerged as pH was raised above the pI, and diminish when the pH was increased further. Small-Angle Scattering (SAS) measurements supported this trend: at the optimum, the data indicated a transition from particulate to fibrillar aggregation, accompanied by enhanced clustering and nano-alignment. At higher pH, the clustering strength and nematic order decreased, consistent with stronger inter- and intra-fibrillar electrostatic repulsion that limits the formation of a cohesive network. Additionally, the primary stabilising interactions were shown to vary with pH (Li et al., 2026). Extrudates produced at pH 7 exhibited a more anisotropic structure compared to those prepared at pH 3 or 5. This was attributed to lower end-barrel viscosity, which allowed for extensive melt deformation together with a protein network stabilised by disulphide bonds. As pH decreased, the network increasingly relied on non-covalent interactions and the contribution of disulphide bonds diminished. This shift in interaction type aligns with compositional effects: using blends of the 7S- and 11S-globulin-enriched fractions (7SF:11SF), Verfaillie, Li, Janssen, et al. (2024) reported that the 7S:11S globulin blending ratio strongly affected processing stability and the development of anisotropy. Particularly, HME processing of samples low in 7SF (0 and 25%; 7S:11S globulin ratios of $\sim$ 0.14 [$\approx$ 12% 7S globulin of total 7S+11S] and 0.26 [$\approx$ 21% 7S globulin of total 7S+11S]) resulted in die pressure fluctuations and led to extrudates with irregular structure, whereas formulations richer in 7SF (50%–100%; 7S:11S globulin ratios $\sim$ 0.42 [$\approx$ 30%], 0.65 [$\approx$ 39%], 1.01 [$\approx$ 50%]) showed a layered structure and similar texture. These trends were linked to differences in protein dispersibility and water holding capacity (WHC), as well as differences in the interactions occurring during processing: in 11SF-based extrudates, a considerable amount of 11S globulins participated in the formation of new disulphide bonds, while in 7SF-based extrudates, the relative contribution of non-covalent interactions was higher than that of disulphide bonds. Complementary findings were reported by Fei et al. (2026), who studied commercial SPIs differing in their 7S:11S globulin ratios. They observed that extrudates prepared from SPI with an intermediate 7S:11S globulin ratio of $\sim$ 0.64 ($\approx$ 39% 7S globulin of total 7S+11S) displayed the most pronounced fibrous structure. At lower and higher ratios, the extrudates were less anisotropic. Specifically, at a 7S:11S globulin ratio of $\sim$ 0.32 ($\approx$ 24% 7S globulin of total 7S+11S), HM extrudates were non-filamentous, whereas at a higher ratio of $\sim$ 0.75 ($\approx$ 43% 7S globulin of total 7S+11S), extrudates exhibited a filamentous but more loosely connected structure. These results indicate that a balanced contribution of 7S and 11S soy globulins is required for the formation of anisotropic fibrous structure under HME. Taken together, these studies show that pH and composition determine the aggregation route and, consequently, the resulting structure formed under HME conditions. However, studies that relate gelation pathways to structure formation under HME under matched pH and composition are lacking.

The aim of this study was, therefore, to determine how pH and the 11S:7S globulin blending ratio govern the aggregation pathway and heat-set gelation of fractionated soy globulins under controlled, non-extruder conditions, and how these behaviours relate to the multiscale structure formed under HME. For this, we first characterised the rheological properties of pH-shifted 11SF and 7SF heat-set gels and related them to the structural changes from the nm- to μm scale probed by SAS. To isolate composition effects, we then prepared gels at pH 7 with 11SF:7SF ratios from 100:0 to 0:100 (w/w) and characterised them in the same way. Finally, to connect gelation behaviour with structure formation under HME conditions, we acquired SANS data on extruded at pH 7 11SF:7SF blends prepared at the same ratios.

2. Materials and methods

2.1. Materials

Commercial semi-defatted soy flour SOYPRO® HP, reportedly defatted by gentle mechanical pressing, without the use of solvents, was obtained from Soy Austria GmbH (Austria); its compositional data are reported in Table S1. Soybeans used are from the Lenka variety, harvested in 2021 in Belgium, and were obtained from Arvesta (Belgium). Sodium dihydrogen phosphate dihydrate, sodium dodecyl sulfate (SDS) and urea were purchased from VWR International (Belgium); calcium chloride dihydrate was from CHEMLAB (Belgium); sodium hydroxide and hydrochloric acid were from Sigma-Aldrich (Germany). All other chemical solvents and reagents were obtained from Merck (Germany).

2.2. Fractionation of 11S and 7S soy globulins

The fractionation of 11S and 7S soy globulins was performed on both laboratory and pilot scale using a common pH-based precipitation method (Nagano et al., 1992). Briefly, soy proteins were extracted at pH 7.5, and 11S- and 7S-globulin-enriched fractions were sequentially precipitated by stepwise pH adjustment to 6.4 and 4.8, respectively, followed by centrifugation and freeze-drying. For the lab-scale procedure (Wu et al., 1999), commercial semi-defatted soy flour was used as the starting material, while for the pilot-scale procedure, soybeans were dehulled, conditioned and flaked, milled to full-fat flour, and solvent-defatted with ethyl acetate prior to extraction (Verfaillie, Li, Janssen, et al., 2024). The resulting fractions are further referred to as 11SF LS and 7SF LS for the lab-scale (LS) fractions, and 11SF PS and 7SF PS for the pilot-scale (PS) fractions. For PS fractions, the fibre and lipid contents were quantified according to the methods described in Merkx et al. (2018) and Hatzakis et al. (2011), respectively: the fibre content was below the detection limit (LOD = 0.1% w/w), and only low lipid levels ($\approx$ 0.1% w/w free fatty acids and diglycerides) were detected in both 11SF PS and 7SF PS. Given the similar fractionation procedure for LS and PS, we expect the residual fibre and lipid content in the LS fractions to be comparable to those of the PS fractions.

2.3. Characterisation of fractionated 11S and 7S soy globulins

2.3.1. Protein composition

The protein contents and compositions were determined for both LS and PS protein fractions. The total protein content in PS fractions was measured in triplicate using the Kjeldahl method according to the ISO 8968-1|IDF 20-1:2014 standard. The protein content of the LS fractions was determined by DUMAS, using an N-factor of 5.7. Protein composition of both PS and LS fractions was assessed by SE-HPLC after extraction in phosphate buffer (pH 6.8) containing urea, SDS, and DTT, as described in Verfaillie, Li, Van Droogenbroeck, et al. (2024).

2.3.2. Zeta potential

Zeta potential (ζ-potential) measurements were performed using a Zetasizer Nano ZS (Malvern Instruments, UK). PS protein dispersions (1% w/w) were prepared in demineralised water and stirred at room temperature for at least 1 h to ensure full hydration. The pH of the dispersions was adjusted to values ranging from ca. 3.0 to 8.0 with 0.1 M HCl or 0.1 M NaOH. After adjusting the pH, the dispersions were left to stand for 1–3 h at room temperature to allow equilibration before analysis. If visible precipitation occurred during this period, the dispersions were allowed to settle, and the supernatant was used for ζ-potential measurements. Measurements were conducted in triplicate at 25 °C, and ζ-potential values were calculated from electrophoretic mobility using the Henry equation with the Smoluchowski approximation.

2.4. Preparation of pH-shifted dispersions and gels

Samples of both LS and PS protein fractions were suspended in demineralised water to a final concentration of 12% w/w and stirred for at least 1 h at room temperature. To investigate the effect of pH on aggregation and gelation, the pH of 11SF and 7SF protein dispersions was adjusted to values ranging from ca. 3.0 to 8.6 using 0.1 M HCl and 0.1 M NaOH. To assess the effect of protein composition, blends of 11SF PS and 7SF PS were prepared at weight ratios of 100:0, 75:25, 50:50, 25:75, and 0:100, but only at neutral pH. Gelation was induced by heating each dispersion at 95 °C for 1 h in a water bath (Julabo). Immediately after heating, the samples were transferred to an ice bath for 15 min and subsequently stored at 4 °C for 1–5 days before they were analysed.

2.5. High-moisture extrusion processing

HME experiments were performed as described in Verfaillie, Li, Janssen, et al. (2024), using a co-rotating twin-screw extruder (Process 11, Thermo Fisher Scientific) with a cooled slit die with inner dimensions of 125 ×19 × 4 mm. Briefly, pre-hydrated blends of 11SF PS and 7SF PS prepared at neutral pH at weight ratios of 100:0, 75:25, 50:50, 25:75, and 0:100 were extruded at a total moisture content of 60% (w/w). The screw speed was set at 600 rpm, and barrel segments 2–7, as well as the die adaptor, were respectively set to 40–60–80-100-120-140-140-140 °C. A total feed rate of 990 g/h was maintained for all extrusion trials. Samples were collected after stabilisation of the die pressure, vacuum sealed and stored at −20 °C.

2.6. Rheological measurements

Rheological measurements were performed on the gel samples differing in pH and protein composition. After equilibration at room temperature for 1 h, the gels were loaded onto an MCR 301 rheometer (Anton Paar, Germany) equipped with a parallel plate geometry (25 mm diameter) and compressed to a fixed gap of 1 mm. Strain sweep tests (0.01%–50% strain, 1 Hz) were conducted at 20 °C, during which the storage modulus (G') and loss modulus (G'') were recorded.

2.7. Small-angle scattering (SAS)

2.7.1. (Ultra-)small-angle X-ray scattering ((U)SAXS)

SAXS and USAXS measurements were performed on the ID02 beamline of the European Synchrotron Radiation Facility (ESRF, Grenoble, France) (Narayanan et al., 2022). Samples were 12% (w/w) dispersions and heat-set gels of the 11SF LS and 7SF LS fractions at pH 4.2, 5.5, 7.2 and 8.6, loaded in 2 mm polycarbonate capillaries. Using the evacuated detector tube, the sample-to-detector distance (SDD) was switched between 1, 8, and 30.9 m, covering a Q range of 0.0002–0.8 Å^{-1} with an X-ray wavelength of 1.014 Å. Data were reduced and placed on an absolute scale (cm^{-1}) with the ID02 pipeline (Narayanan et al., 2022). The instrument-specific software SAXSutilities (Sztucki, 2021) was used for background subtraction of water-filled capillaries, merging measurements recorded at different SDDs and other specific operations.

Depending on the sample, the scattering profiles were described with either (i) a two- or three-level Unified Beaucage (UB) model or (ii) a Broad Peak (BP) model, using SasView software (Doucet et al., 2025).

Unified Beaucage (UB). For each structural level i, the UB intensity is the sum of a Guinier term and a power-law term (Beaucage, 1995, 1996):

$$I(Q) = \sum_{i=1}^{N}\left[G_i \exp\left(-\frac{Q^2 R_{gi}^2}{3}\right) + B_i \frac{\left(\mathrm{erf}(QR_{gi}/\sqrt{6})\right)^{3n_i}}{Q^{n_i}}\right] + \mathrm{bkg}. \quad (1)$$

Here, $G_i = c_i V_i \left(\Delta \mathrm{SLD}_i\right)^2$ is the Guinier prefactor (V_i the particle volume and $\Delta\mathrm{SLD}_i$ the scattering length density contrast), R_{gi} is the radius of gyration describing the average size of the ith structural feature, B_i is the prefactor of the power-law with exponent n_i, and bkg is a background. Two or three levels were used depending on the sample. For the largest-scale level, only a power-law was fitted; R_{gi} was fixed to 50000 Å ($\gg Q_{\min}^{-1}$). For cross-sample comparison, we report a clustering strength (CS) from the UB model, B_1/Q^{n_1} evaluated at $Q = 0.0005$ Å^{-1} (μm-scale features).

Broad Peak (BP). The BP model is described by the following equation:

$$I(Q) = \frac{A}{Q^n} + \frac{C}{1 + (|Q - Q_0|\,\xi)^m} + \mathrm{bkg} \quad (2)$$

The first term A/Q^n describes the low-Q power-law decay from the large-scale structures; the second is a Lorentzian-type feature with correlation length (CL) ξ, shape exponent m and peak/shoulder position Q_0; bkg represents background. For BP, we define CS analogously as A/Q^n at $Q = 0.0005$Å^{-1}.

2.7.2. Small-angle neutron scattering (SANS)

SANS measurements were performed on the Larmor Instrument at the ISIS Neutron and Muon Source (STFC Rutherford Appleton Laboratory, UK) (ISIS Larmor). The time-of-flight configuration provided a simultaneous Q range of 0.005–0.7 Å^{-1} using incident wavelengths 0.9-13 Å. Heat-set gels of 11SF PS and 7SF PS were measured across pH 3.0–7.8 (step 0.8) and, at pH 7.0, for blends with 11SF PS:7SF PS blending ratios (w/w) of 100:0, 75:25, 50:50, 25:75, and 0:100. Extrudates of the same compositions were also measured with the extrusion direction known. Samples were mounted in demountable gel cells with quartz windows and measured with a symmetric squared sample aperture (5 x 5 mm^2) at ambient temperature.

Two-dimensional data were reduced in Mantid (Arnold et al., 2014), placed on an absolute intensity scale (cm^{-1}) by measuring the scattering of a mixture of hydrogenous and deuterated polystyrene with a known radius of gyration and scattering cross-section (Wignall & Bates, 1987), and corrected for detector sensitivity. The scattering background of the quartz windows was subtracted. Isotropic gel data were radially averaged. For anisotropic extrudates, sector averages of width ±15° were taken parallel (‖) and perpendicular (⊥) to the extrusion direction.

Table 1
Composition and total protein of 11S- and 7S-enriched soy globulin fractions prepared at lab scale (LS) and pilot scale (PS).

Fraction	Scale	Protein (%DM)	11S (%)	7S (%)	2S (%)
11SF	LS	86*	79	13	8
	PS (Verfaillie, Li, Janssen, et al., 2024)	91*	77	10	11
7SF	LS	89*	30	58	9
	PS (Verfaillie, Li, Janssen, et al., 2024)	87*	39	39	14

*Note that protein %DM was quantified by DUMAS method for LS fractions and by Kjeldahl method for PS fractions.

Isotropic gel data were primarily used to classify scattering behaviour (from the overall power-law character and the presence/position of a mid-Q shoulder). When a distinct mid-Q shoulder was present, the data were fitted in SasView (Doucet et al., 2025) with the Correlation Length model (Hammouda et al., 2004):

$$I(Q) = \frac{A}{Q^n} + \frac{C}{1 + (Q\xi)^m} + \text{bkg.} \quad (3)$$

where A is the power-law scale factor, n is the power-law exponent, C is the Lorentzian scale factor, ξ is the Lorentzian correlation length (CL), m refers to the exponent of the Lorentz function, bkg is the flat background that accounts for incoherent scattering.

Sector-averaged extrudate data were fitted separately (∥ and ⊥) with a two-level UB model (Eq. (1)). In addition, annular intensity averages over a fixed Q-range ($0.005 < Q < 0.06 Å^{-1}$) were obtained from the anisotropic extrudate data and fitted with a Legendre series expansion to extract the nematic order parameter as outlined elsewhere (Garina et al., 2024; Kuijpers et al., 2025).

3. Results and discussion

3.1. Characterisation of fractionated 11S and 7S soy globulins

Protein content and composition of the 11SF and 7SF fractions prepared at LS and PS are summarised in Table 1. Across all four materials, total protein content fell within 86%–91% of dry matter (DM). For 11SF, both LS and PS batches predominantly contained 11S globulins with a minor content of 7S globulins (79/13% and 77/10%, respectively). For 7SF, the target 7S globulin component dominated, but substantial 11S globulin remained, with 7S = 58% (LS) and 39% (PS), and 11S = 30% (LS) and 39% (PS). Overall, the composition of the 11SF and 7SF fractions obtained at both scales was comparable, supporting the joint interpretation of the LS and PS datasets in the sections that follow, where LS data are used alongside PS only for the pH series, while the results of blending experiments at pH 7 are presented for the PS fractions only.

Fig. 1 shows zeta potential results for 11SF PS and 7SF PS dispersions. Because the globulins in the 7S- and 11S-globulin-enriched fractions have largely retained their native form (Section 3.2.2), their solubility is expected to be governed by thermodynamic equilibrium between dissolved and precipitated states (Gao et al., 2024). Under these conditions, we assume that there is no difference in conformation or net charge between soluble and precipitated 7S and 11S globulins. Therefore, we interpret the measured ζ-potential values of the electrophoretically mobile fraction as representative of the overall pH-dependent charge state of globulins in the system. Within this framework, ζ-potential decreases from ~+25–30 mV at pH ~3 to negative values above pH ~5. The zero-mobility points ($\zeta = 0$) occur at pH ~4.90 for 7SF and pH ~5.10 for 11SF. These values are close to the literature pI values reported by Koshiyama (1968, 1972), with small offsets expected from methodological and/or compositional differences. Above the pI, $|\zeta|$ increases more rapidly with pH for 7SF than for 11SF, indicating a steeper buildup of negative surface potential for 7S under tested conditions.

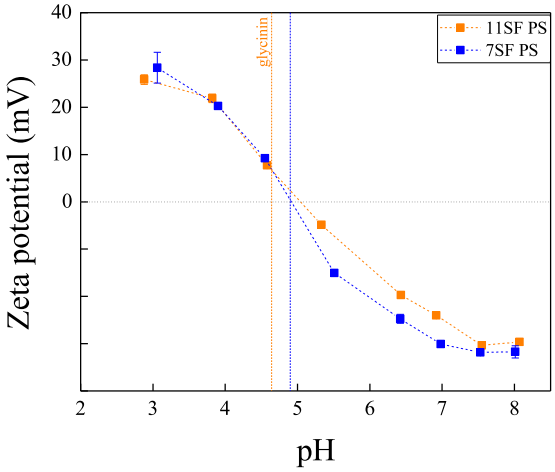


Fig. 1. Zeta potential values obtained for 11SF PS and 7SF PS 1% (w/w) dispersions as a function of pH. Error bars refer to triplicate measurements. Vertical lines indicate pI values for glycinin and β-conglycinin from literature (Koshiyama, 1968, 1972). The compositions of the 11SF and 7SF fractions, reflecting the actual 11S and 7S globulin ratios in the enriched fractions, are given in Table 1.

3.2. Effect of pH on gel formation

3.2.1. Visual appearance and rheological properties

The visual appearance of the heat-set gels provides a first qualitative indication of the network structures formed as a function of pH (Fig. 2A). For both 11SF PS and 7SF PS, a non-monotonic effect of pH is observed. Near the isoelectric region, the gels appear opaque and granular, with visible separation into protein-rich and protein-poor regions. At pH values further from the pI, the gels become more homogeneous and translucent. Such changes in appearance are commonly associated with differences in aggregation behaviour during heat-set gelation: near the pI, reduced electrostatic repulsion favours extensive, random aggregation and formation of particulate gels, whereas at pH further from the pI, increased surface charge limits aggregate growth and promotes more ordered, fine-stranded aggregation (Doi, 1993; Khalesi et al., 2024).

These qualitative differences are reflected in the rheological response of the gels (Fig. 2 B, strain sweeps for each measurement are presented in Fig. S1). Both 11SF PS and 7SF PS exhibit a maximum in storage and loss moduli (G' and G'') close to their respective pIs, followed by a pronounced decrease when moving to either more acidic or more alkaline pH. Such pH-dependent rheological trends are expected and in agreement with previous studies on soy globulins and SPI gels (Lakemond et al., 2003; Nagano et al., 1994; Renkema et al., 2002, 2001). Gel stiffness is typically related to protein solubility during heating (Renkema et al., 2002, 2000). It is generally assumed that protein remaining dissolved after heating is not incorporated into the network, in contrast to precipitated polypeptides and subunits. Consequently, lower concentrations of aggregated protein available for network formation result in a lower stiffness of the gels.

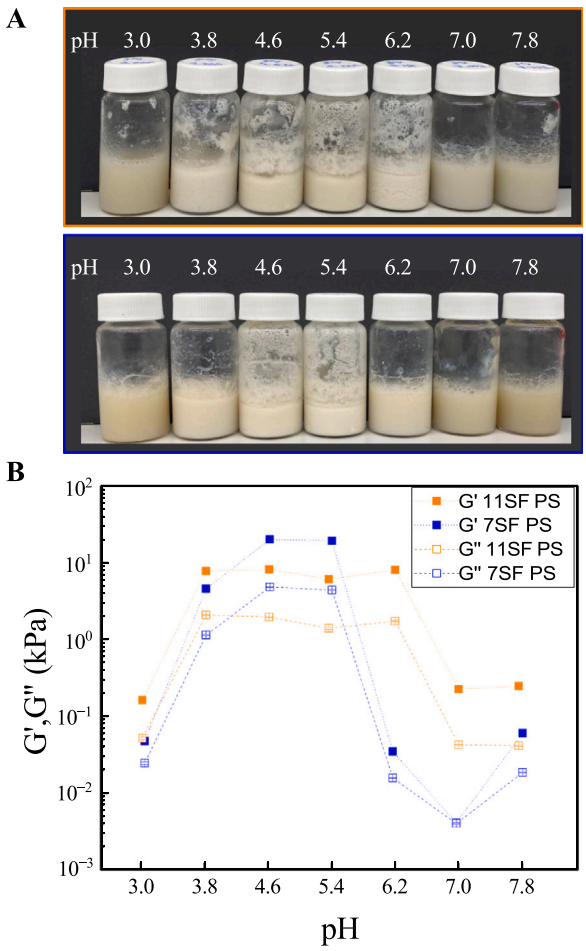


Fig. 2. Effect of pH on: (A) the visual appearance of gels prepared from 11SF PS (orange frame) and 7SF PS (blue frame); and (B) the storage modulus (G') and loss modulus (G") of 11SF PS and 7SF PS gels. Rheology data for LS gels are shown in Fig. S3. The compositions of the 11SF and 7SF fractions, reflecting the actual 11S and 7S globulin ratios in the enriched fractions, are given in Table 1.

In this sense, literature data on globulin solubility support the observed rheological trends. Reported solubility data for 7S- and 11S-enriched fractions obtained using similar fractionation procedure show that both 7S and 11S globulins exhibit the characteristic U-shaped pH-solubility profiles, with minimum solubility near the pI (Jiang et al., 2010). However, the width of this low solubility region differs between the two globulins: 7S globulins exhibit a relatively narrow pH range of minimum solubility, whereas 11S globulins remain poorly soluble over a broader pH interval. At higher pH, 7S globulins are generally more soluble than 11S globulins. These literature-reported solubility trends are also consistent with the visual appearance of our dilute (1 wt%) PS dispersions after pH adjustment (Fig. S2), which show a broader low-solubility region for 11SF PS than for 7SF PS. In line with these solubility trends, the present rheological data show that 7SF PS exhibit a narrow pH range over which maximum G' is observed, while 11SF PS maintains elevated G' values over a broader pH range and remains stiffer than 7SF further away from the pI. The LS gels show comparable pH-dependent trends (Fig. S3), supporting the joint interpretation of LS and PS data in the subsequent sections.

At the same time, the present results demonstrate that solubility trends cannot be directly inferred from zeta potential alone. In general, a decrease in $|\zeta|$ is associated with reduced electrostatic repulsion and a higher tendency to aggregate. However, at pH 6.2, the measured $|\zeta|$ for both 11SF and 7SF are comparable (Fig. 1), yet literature data indicate markedly different solubilities for the two globulins under these conditions (Jiang et al., 2010), and the corresponding G' values remain substantially different (Fig. 2 B). This suggests that zeta potential provides only a partial description of aggregation behaviour and that protein-specific factors such as molecular size, hydrophobic interactions, and crosslinking capacity should be taken into consideration. We hypothesise that the larger 11S globulin, which has greater hydrophobic exposure upon heating and a higher cysteine content, can sustain aggregation and network formation even at relatively high net charge, resulting in lower solubility and higher gel stiffness over a broader pH range. In contrast, the smaller 7S globulin, with lower crosslinking capacity and generally higher $|\zeta|$, exhibits a narrower range of conditions under which extensive aggregation occurs.

It is also important to note that previous studies have shown that gel stiffness does not uniquely reflect the amount of aggregated protein, but also strongly influenced by the architecture of the resulting network (Doi & Kitabatake, 1989; Renkema, 2004; Renkema et al., 2002). In a recent study combining rheology and SAS, Tiong et al. (2025) demonstrated that protein gels formed from isolates with different solubilities can develop distinct network structures while exhibiting similar storage moduli, and that both soluble and insoluble proteins may contribute to gelation depending on the aggregation pathway. These findings emphasise that a mechanistic understanding of gelation behaviour requires direct insight into aggregate morphology, connectivity, and spatial organisation across length scales.

For applications such as meat alternatives, this distinction is particularly important. In our previous work on pH-shifted HME (Kuijpers et al., 2025), we showed that differences in aggregation pathway govern the development of multiscale anisotropic structures under flow. This motivates a structural analysis beyond solubility considerations, focusing on the multiscale organisation of aggregates formed as a function of pH, which is addressed in Section 3.2.2 and Section 3.2.3.

3.2.2. *Multiscale structure of dispersions and gels by (U)SAXS*

To examine multiscale structural changes upon gelation across different pH values, we collected (U)SAXS data on the LS fractions at four representative pH values. For each pH, the same formulation was measured both as a dispersion and as a heat-set gel, allowing for a direct before-and-after comparison of structural signatures. The resulting profiles are presented in Fig. 3.

In the high-Q region ($Q > 0.06$ Å^{-1}), dispersions of both 11SF LS and 7SF LS show clear form factor oscillations of native soy 11S and 7S globulins. A pronounced maximum at $Q \approx 0.12$–0.13 Å^{-1} (red arrows in the Kratky plots, Fig. 3, right) is accompanied by a broader shoulder at $Q \approx 0.06$–0.07 Å^{-1} (green arrows). CRYSOL (Svergun et al., 1995) calculations based on the PDB assemblies (11S soy globulin, 1OD5; 7S soy globulin, 1FXZ) reproduce this shoulder–peak pair (Fig. S4). The shoulder reflects the overall hexamer or trimer dimensions (ca. 10 nm), while the high-Q maximum corresponds to a subunit-scale intra-oligomer spacing (ca. 5 nm). Upon heating to form gels, the high-Q oscillations vanish and the remaining high-Q shoulder shifts towards lower Q. This behaviour is consistent with the loss of well-defined intraparticle distances due to (partial) unfolding and aggregation, together with an increase in the effective size of the scattering entities.

In the mid-Q region ($0.002 < Q < 0.07$Å^{-1}), a shoulder-like feature (purple arrows in the Kratky plots, Fig. 3, right) is evident in dispersions measured away from the pI. We attribute this feature to an interplay between electrostatic repulsion and short-range attraction (Stradner et al., 2006). At pH > 7, where both proteins carry a high net charge, the shoulder is narrow and high, indicating repulsion-dominated order with limited attraction (Chinchalikar et al., 2013; Weijers et al., 2005). The shoulder occurs at ca. 0.035 Å^{-1} for 7SF dispersions and at ca. 0.015–0.020 Å^{-1} for 11SF dispersions, reflecting the formation of finer-scale aggregates in 7S-enriched soy globulin fractions (Renkema et al.,

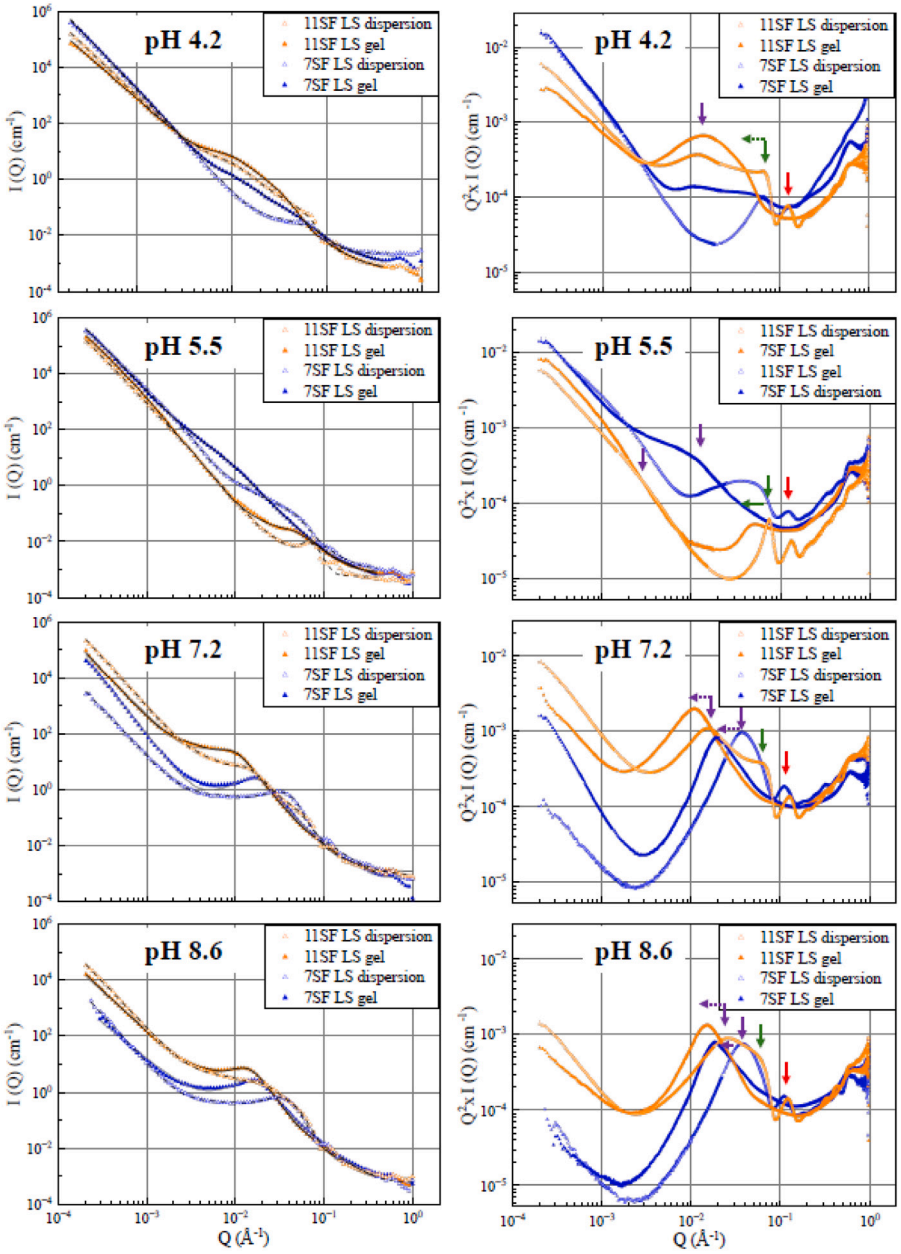


Fig. 3. (U)SAXS profiles of 11SF LS and 7SF LS dispersions and gels at different pH values. (Left) Log–log plots showing experimental data (symbols) and corresponding model fits (lines). Fits were obtained using the Unified Beaucage (UB) model (Eq. (1)) (black) and, where applicable, the Broad Peak model (Eq. (2)) (grey). (Right) Corresponding Kratky plots of experimental data, highlighting key structural features: high-Q form factor peak (red arrows), high-Q form factor shoulder (green arrows), and mid-Q shoulder arising due to repulsive and/or attractive interactions (purple arrows). The compositions of the 11SF and 7SF fractions, reflecting the actual 11S and 7S globulin ratios in the enriched fractions, are given in Table 1.

2001). As pH approaches the pI, attraction becomes more prominent and the feature becomes broader and less pronounced, consistent with particulate aggregation. The same characteristic mid-Q shoulder-like feature persists in the gelled samples. At pH > 7, the mid-Q shoulder becomes narrower while shifting towards lower Q (11SF: ca. 0.015–0.020 $Å^{-1}$ in dispersions → ca. 0.011–0.012 $Å^{-1}$ in gels; 7SF: ca. 0.035 $Å^{-1}$ in dispersions → ca. 0.019 $Å^{-1}$ in gels), indicating that heating promotes short-range attraction through (partial) unfolding and crosslinking, allowing strands/clusters to grow and reorganise, which increases the characteristic spacing and reduces positional disorder (Weijers et al., 2005). As pH approaches the pI, the shoulder remains visible but becomes broader with a modest shift, and the mid-Q intensity rises, reflecting stronger attractive interactions after heating. In the lowest-Q region ($Q < 0.002 Å^{-1}$), all profiles exhibit a power-law upturn, indicating large-scale heterogeneity consistent with fractal-like aggregates or network domains on the sub-μm to μm scale (Tiong et al., 2025).

To enable quantitative comparison of the pH trends in dispersions and gels, (U)SAXS data were fitted with the UB model (Eq. (1)) using two or three structural levels (all fitting parameters are shown in Table S2.1). For most samples, the UB model provided an adequate description across the usable Q range and reproduced the mid-Q shoulder (black lines in Fig. 3, left); deviations at high Q in dispersions are expected because the UB model does not reproduce molecular form factor oscillations. For the 7SF LS gels at pH > 7, however, the UB model did not describe well the mid-Q correlation feature, so these datasets were additionally fitted with the BP model. For consistency within the high-pH gel set, the 11SF LS gels at pH > 7 were also fitted

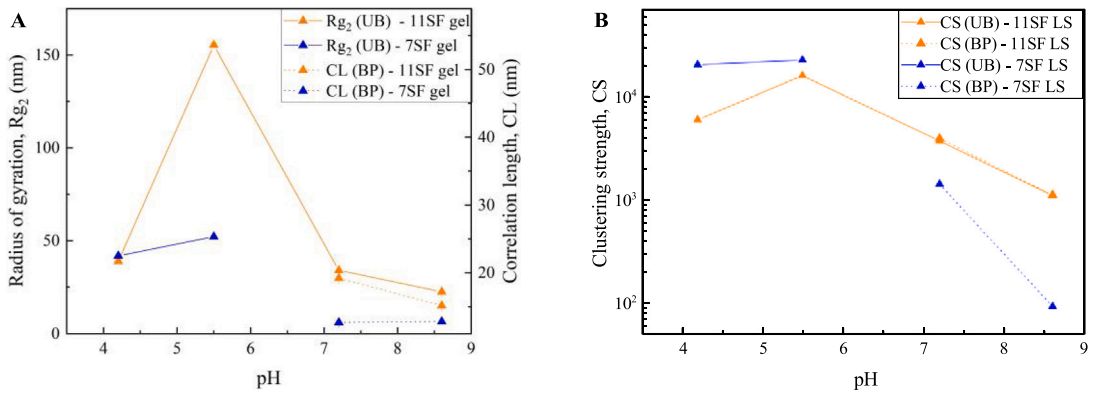


Fig. 4. Effect of pH on mid-scale characteristic size reported as radius of gyration of intermediate-scale structures (Rg_2) and/or correlation length (CL) (A) as well as clustering strength (CS) obtained from (U)SAXS data. (B) for 11SF LS and 7SF LS gels. Rg_2 and CL values are obtained from Unified Beaucage (UB) (Eq. (1)) and Broad Peak (BP) (Eq. (2)) fits, respectively. CS is calculated as B_1/Q^{n_1} for UB fits and A/Q^n for BP fits (Section 2.7). The compositions of the 11SF and 7SF fractions, reflecting the actual 11S and 7S globulin ratios in the enriched fractions, are given in Table 1.

with the BP model (Eq. (2)) (all fitting parameters are shown in Table S2.2) alongside the UB model (grey lines in Fig. 3, left).

Although the UB model does not accurately reproduce the high-Q molecular form factor oscillations, inspection of the fits (Table S2.1) shows that all dispersions and gels required a high-Q UB level (reported as Rg_3) to capture small-scale structure. Rg_3 lies in the few nm (ca. 3–8 nm) range, indicating that even after gelation, somewhat compact globular protein units persist, consistent with SAXS studies by Guo et al. (2012), Xiao et al. (2016), who likewise reported that soy globulins maintain their globular shape even after heating. Thus, gels still contain nm-scale building blocks, while larger-scale features are captured by the intermediate and low-Q levels.

When comparing the Rg_2 values (Table S2.1), which describe the mid-Q scattering, before and after heating, it becomes evident that for 11SF LS at high pH, Rg_2 increases (e.g., ca. 24 nm → 34 nm at pH 7.2; ca. 15 → 22 nm at pH 8.6), consistent with the associated growth of strands during heating. At pH 4.2, the change in Rg_2 after heating is modest (ca. 32 nm → 39 nm). Near the pI (pH 5.5), Rg_2 decreases (ca. 246 nm → 155 nm), while the low-Q intensity grows, indicating that more contrast resides at the largest scales in the gel. As a result, the mid-Q shoulder-like feature is less well-defined, and the fitted Rg_2 should be interpreted with caution. For 7SF LS, Rg_2 at low pH is essentially unchanged by gelation (ca. 51 nm → 52 nm at pH 5.5) and becomes defined in the gel at pH 4.2 (ca. 42 nm). At pH > 7, the gel mid-Q feature is not adequately captured by the UB model and is treated with the BP model. This difference in fitting approach prevents a direct numerical comparison between the UB-derived Rg_2 values for dispersions and the BP-derived CL values for gels. Nevertheless, within the dispersions the UB fits show larger Rg_2 for 11SF than for 7SF (e.g., ca. 24 nm for 11SF vs ca. 8 nm for 7SF at pH 7.2; ca. 15 for 11SF vs ca. 8 nm for 7SF at pH 8.6), consistent with the mid-Q shoulder appearing at lower Q in 11SF than in 7SF (Fig. 4) and with the formation of thicker strands by the cysteine-rich 11S globulins.

For the gels, Fig. 4A summarises the mid-scale characteristic sizes obtained from the fits: Rg_2 when the UB model describes the scattering data (all pH < 7 and also 11SF at pH > 7), and the CL when the BP model is used (pH > 7). Fig. 4B reports the CS, which we interpret as a measure of the extent of clustering at sub-μm to μm length scales (Hammouda et al., 2004; Kuijpers et al., 2025). In general, both mid-scale characteristic sizes and CS mirror the trends observed for gel appearance and rheology: they peak near the pI, where gels are opaque and G'/G'' are highest, and decrease away from the pI as the gels become weaker and more translucent. These trends are also consistent with literature-reported solubility data for 7S- and 11S-globulin-enriched fractions, which show minimum solubility near the pI and increasing solubility when moving away from it (Jiang et al., 2010). Notably, despite the intrinsic tendency of 11S globulins to form denser aggregates (Guo et al., 2012) and stiffer gels than 7S globulins (Yang et al., 2024), CS is higher for 7SF than for 11SF close to the pI, while the opposite trend is found at pH values further from the pI. This pattern reflects their differences in thermal stability and ability to form intermolecular disulphide crosslinks during heating: at the pI, electrostatic repulsion is minimal, and the 7S globulin, with a lower denaturation temperature (Renkema et al., 2002), unfolds earlier and assembles into numerous compact particulate clusters, increasing the density of mesoscale contacts and yielding higher CS and G'. Under the same conditions, the 11S globulin tends to form larger particulate aggregates, so the number of distinct clusters per unit volume at these scales is lower, and CS correspondingly decreases. At higher pH (pH > 7), strong long-range repulsion imposes a characteristic spacing that, upon heating, 11S globulins can stabilise more effectively through intermolecular disulphide crosslinks. This produces a more cohesive network with thicker strands (Fig. 4A), higher CS (Fig. 4B), and higher moduli (Fig. 2B) compared to 7S globulins, whose hydrophilic extension regions and higher net charge (Fig. 1) sustain repulsion and limit aggregation under the same conditions.

3.2.3. *Multiscale structure of gels by SANS*

To complement the (U)SAXS analysis, SANS measurements were additionally performed on the PS fractions (11SF PS and 7SF PS) for heat-set gels across pH 3.0–7.8. Although the SANS Q range is more limited compared to (U)SAXS (Q_{min} ca. 0.005 Å^{-1} vs 0.0002 Å^{-1}) and the high-Q range is dominated by incoherent background scattering, it still captures the low–mid-Q signatures that are useful to distinguish particulate from fibril-like aggregation. We therefore use SANS primarily to classify the scattering behaviour (from the overall power-law behaviour and the presence/position of a mid-Q shoulder), and, only where a distinct mid-Q shoulder is present, to extract a single characteristic length - CL, obtained from the fit with the Correlation Length model (Eq. (3)), for comparison across pH. The resulting profiles are shown in Fig. 5.

Based on the SANS curve shapes, we distinguish three scattering behaviours across pH: (i) repulsion-dominated (pH 3.0, 7.0, 7.8), (ii) attraction-dominated with residual repulsion (pH 3.8 for both globulin-enriched fractions; pH 6.2 for 7SF), and (iii) strong attraction near the pI (11SF and 7SF at pH 4.6 and 5.4; 11SF also at pH 6.2).

For behaviour (i), a clear mid-Q correlation shoulder is present (Fig. 5A,F,G for both 11SF and 7SF). In several cases, an intermediate Q region exhibits a local slope of ca. -1, characteristic of a linear array of scattering centres (fibrillar-/strand-like aggregation). This is most evident at pH 3.0 for both globulin-enriched fractions and becomes particularly well defined for 7SF at pH 7.0 (slope ca. −1.3) and pH 7.8

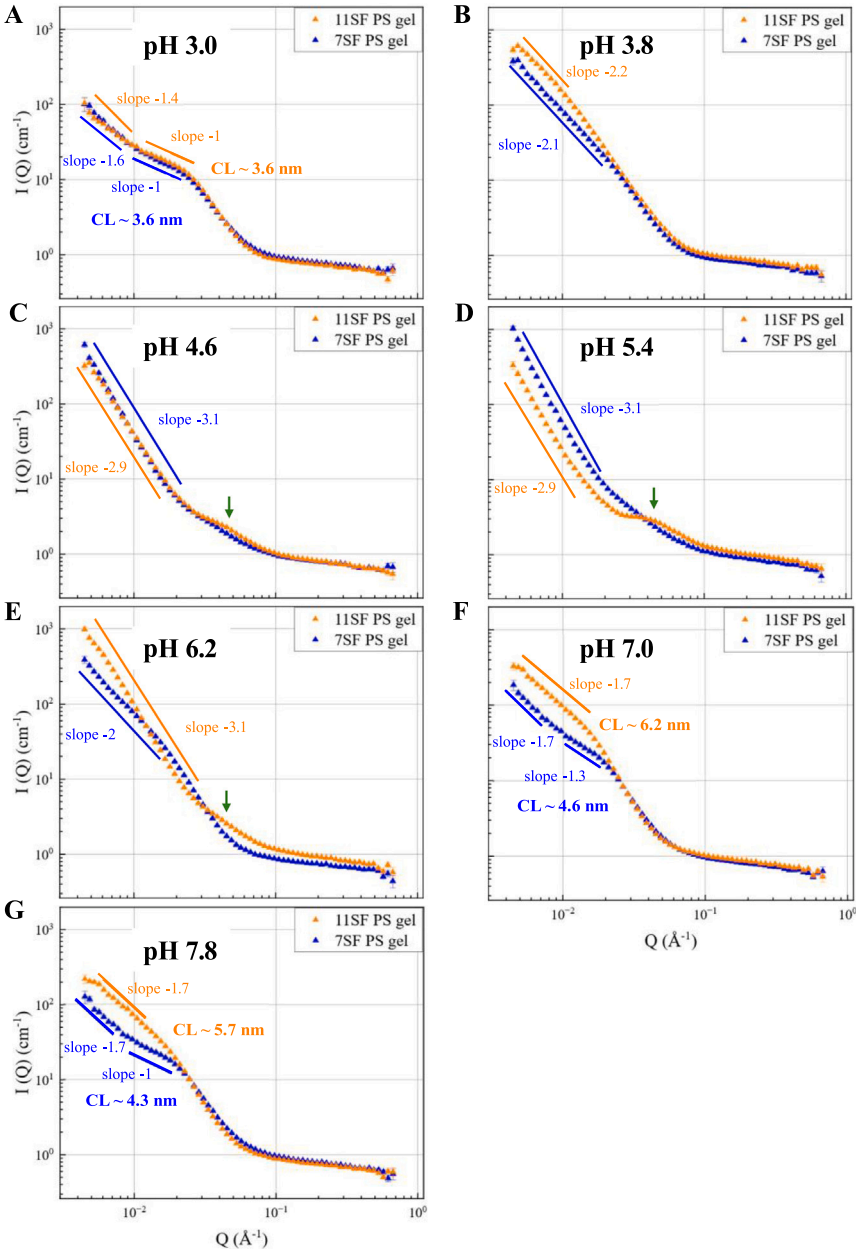


Fig. 5. SANS profiles of 11SF PS and 7SF PS gels at different pH values. Where present, green arrows in panels C–E indicate high-Q form factor shoulders. The compositions of the 11SF and 7SF fractions, reflecting the actual 11S and 7S globulin ratios in the enriched fractions, are given in Table 1.

(slope ca. −1.0), indicating that increasing charge favours more loosely connected linear aggregates. For 11SF at pH ≥ 7, the intermediate band is less isolated and the local slope is steeper (slope ca. −1.7), consistent with more connected and denser strands. For the conditions in (i), we report a CL obtained from the fit with the Correlation Length model (all fitting parameters are shown in Table S3): at pH 3.0, CL ≈ 3.6 nm for both globulin-enriched fractions (Fig. 5A); at pH 7.0, CL ≈ 6.3 nm (11SF) and ≈ 4.6 nm (7SF) (Fig. 5F); at pH 7.8, CL ≈ 5.7 nm (11SF) and ≈ 4.3 nm (7SF) (Fig. 5F). Thus, at high pH, the characteristic length is larger for the 11S globulin, in line with the SAXS mid-scale lengths and the higher moduli of 11SF gels away from the pI (Fig. 2).

For behaviour (ii), the shoulder is broad and weak, and the slopes steepen towards ca. -2, indicating denser, particulate-type aggregation rather than strands (Fig. 5B for both 11SF and 7SF and Fig. 5E for 7SF). For 7SF, the shoulder is more apparent at pH 6.2 than at pH 3.8, pointing to a greater repulsive contribution at pH 6.2 (Fig. 1). Correspondingly, the gels are weaker at this pH, matching the rheology results (Fig. 2).

For behaviour (iii), the profiles show a form factor shoulder (green arrows) followed by a steep slope of ca. −3 (Fig. 5C,D for both 11SF and 7SF and Fig. 5E for 11SF), consistent with particulate aggregation near the pI. This regime coincides with the maxima in G' and G'' and with opaque, phase-separated gels. The pH interval over which (iii) appears is broader for 11SF than for 7SF, mirroring the rheological trends (Fig. 2).

Taken together, the (U)SAXS/SANS results on heat-set gels reveal structural features similar to those previously identified in pH-shifted HME of soy proteins (Kuijpers et al., 2025). At the lowest structural level, both gels and extrudates comprise somewhat compact protein units that are likely moderately unfolded yet still retain globular shape (Guan et al., 2024). These somewhat compact proteins persist after heating and under HME conditions (Garina et al., 2024, 2026;

Guan et al., 2024), serving as the elementary building blocks from which strands and nano-aggregates form.

At higher structural levels, the same three pH-dependent regimes emerge. Near the pI, aggregation is particulate: the mid-Q shoulder collapses, and the mid/low-Q range is power-law dominated, matching the opaque, phase-separated gels here, and, in extrudates, increased sub-mm disorder and low anisotropy. As pH moves further from the pI, a balance of electrostatic repulsion and attraction leads to strand/fibril-like aggregation: a clear mid-Q shoulder appears and sharpens with rising pH, coinciding, under HME, with the emergence of lamellar phase separation and maximal anisotropy. At most alkaline conditions, electrostatic repulsion prevails: while fibrillar aggregates form, they remain too weakly clustered to create a cohesive network, which is reflected in weak and disordered lamellar development and decreased anisotropy under HME.

Despite this similarity in aggregation regimes, the evolution of mid-scale characteristic sizes diverges between the two systems. In HM extrudates, the CL, defined as the size of the smallest discernible scattering object, and the size of nano-aggregates increase as pH rises above the pI. In contrast, in gels, the mid-scale characteristic size (CL or Rg_2) decreases under the same conditions. These opposing trends likely arise from the different conditions under which aggregation occurs during static heating versus extrusion, and this is discussed in detail in Section 3.4.

Nonetheless, our findings demonstrate clear parallels between gelation and extrusion, indicating that the formation of structure during HME and gelation is governed by the same pH-induced charge effects that control protein-protein interactions. Accordingly, the aggregation behaviour observed during heating serves as a useful indicator of trends in structure formation during HME, despite the presence of process-specific differences. It should be noted, however, that in our study on the effect of pH shifting on structure of HM extrudates, we used a SPC, where 11S and 7S globulins are present in partially denatured forms. Here we worked with fractionated globulins that largely retained their native structure. For these fractionated proteins, we observe distinct, composition-specific gelation behaviours (e.g., at pH > 7, 11S forms thicker strands with larger spacings and higher CS than 7S). Consequently, when 11S and 7S are present together (as in SPC or SPI), their blending ratio is expected to affect the aggregation behaviour (Guo et al., 2012) and thereby govern the structure formed during HME (Fei et al., 2026; Verfaillie, Li, Janssen, et al., 2024). In the next subsection, we, therefore, examine how composition influences gelation and how these trends relate to structure formation during HME under neutral pH conditions.

3.3. Effect of 11S:7S globulin blending on gel formation

To isolate composition effects at pH 7, we used the same pilot-scale fractions (11SF PS and 7SF PS) as (Verfaillie, Li, Janssen, et al., 2024) to prepare gels at matching 11SF:7SF blend ratios (w/w): 100:0, 75:25, 50:50, 25:75, and 0:100. These gels were characterised by small-amplitude oscillatory rheology and SANS. We also performed SANS on the exact same HM extrudates reported by Verfaillie, Li, Janssen, et al. (2024), enabling a composition-matched comparison between gel behaviour and HM extrudate structure at a fixed formulation and pH.

3.3.1. Rheological properties

To characterise the rheological properties of samples differing in 7S and 11S globulin content, strain sweeps were performed on the prepared heat-set gels. Fig. 6 presents the results, where the bottom axis shows the nominal blend ratios (11SF:7SF, w/w), and the secondary top axis reports the corresponding actual 7S globulin content (as % of total 7S+11S), calculated from the measured compositions in Table 1. The results reveal that the stiffest gel is formed at 100:0 (w/w) 11SF:7SF. Introducing 25% 7SF causes a sharp drop in G'. For ≥50% 7SF, both G' and G'' remain very low and change only marginally with composition.

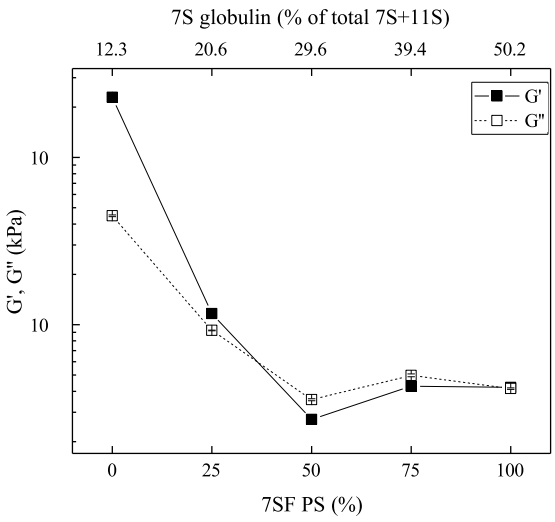


Fig. 6. Effect of 11S:7S globulin blending on the storage modulus (G', closed symbols) and loss modulus (G", open symbols) of PS gel samples at pH 7.0. The bottom axis shows the 7SF PS mass fraction (the remainder is 11SF PS), while the top axis gives the corresponding 7S globulin content (% of total 7S+11S) based on the values obtained for 7SF PS and 11SF PS Table 1.

This trend suggests that the 11S globulin dominates network formation at higher ratios, consistent with the scattering at pH 7: 11SF forms thicker, more tightly connected strands that give rise to networks with higher CS, whereas 7SF forms finer, more weakly connected structures (Fig. 3, Fig. 4, and Fig. 5). Consequently, increasing 7SF content shifts the system towards the low-modulus, 'weak-gel' regime observed for 100% 7SF.

3.3.2. Multiscale structure by SANS

The trends observed in the rheology measurements (Fig. 6) are also mirrored in the SANS intensity profiles (Fig. 7). As the 7SF content increases, the low-Q intensity decreases and the mid-Q correlation shoulder shifts to slightly higher Q (Fig. 7A). The corresponding CL, with all fitting parameters detailed in Table S4, decreases with 7SF content, most sharply from 0 to 25% 7SF, and then tends towards a plateau from 50 to 100% 7SF (Fig. 7B), consistent with the formation of thinner, more irregular strands as 7SF is added (Hermansson, 1985; Renkema et al., 2002). Across the series, the shoulder remains, but the intermediate-Q band becomes progressively more pronounced as 7SF increases. In 11S-globulin-rich gels, it is less isolated with a steeper local slope (ca. −1.7), whereas at 75%–100% 7SF, it approaches −1.3, indicative of more linear, loosely connected aggregates. Notably, the largest change occurs on adding 25% 7SF, after which further increases in 7SF produce only modest additional changes in both intensity and CL, matching the sharp drop in G' between 0% and 25% 7SF and the 'weak-gel' plateau observed for ≥50% 7SF.

3.4. Effect of 11S:7S globulin blending on multiscale structure of high-moisture extrudates

To enable a composition-matched comparison between gel behaviour and HM extrudate structure, we collected SANS data on the extruded 11SF, 7SF, and their blends. To evaluate the nm-scale structural anisotropy in the extrudates, annular intensity averages were fitted with a Legendre series expansion and the nematic order parameter was extracted. Fig. 8 displays the resulting values. The order parameter exhibits a clear maximum at the 50:50 (w/w) blend and remains elevated for 75% and 100% 7SF compared to the 0% and 25% cases. This observation aligns with the findings of Verfaillie, Li, Janssen, et al. (2024), who reported that extrusion of 100:0 and

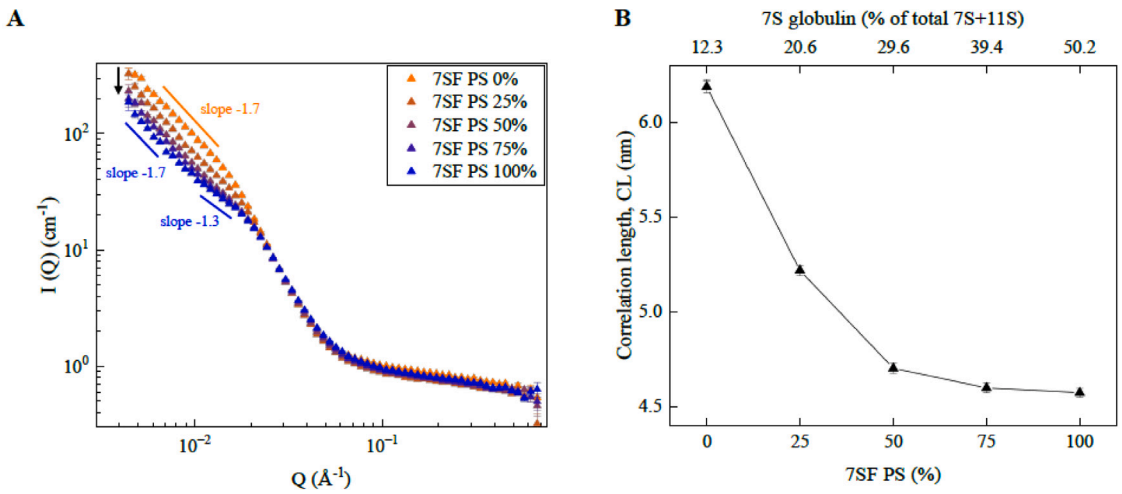


Fig. 7. SANS results from gels prepared from blends of the 7SF PS and 11SF PS at pH 7.0. (A) SANS profiles for gels with increasing 7SF content. Arrow indicate the systematic decrease in low-Q intensity with increasing 7SF content, while slope annotations highlight the progressive change in the intermediate-Q regime. (B) Correlation length (CL) values, obtained by fitting the curves in (A) with the Correlation Length model (Eq. (3)). The bottom axis shows the 7SF PS mass fraction (the remainder is 11SF PS), while the top axis gives the corresponding 7S globulin content (% of total 7S+11S) based on the values obtained for 7SF PS and 11SF PS (Table 1).

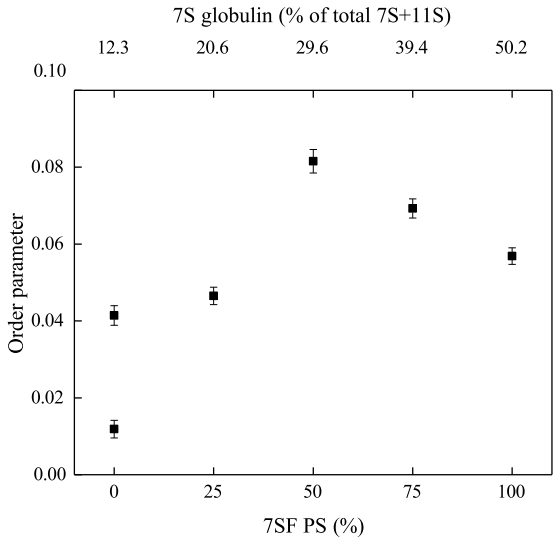


Fig. 8. Degree of nano-alignment in extrudates as a function of blend composition: the bottom axis shows the 7SF PS mass fraction (the remainder is 11SF PS), while the top axis gives the corresponding 7S globulin content (% of total 7S+11S) based on the values obtained for 7SF PS and 11SF PS (Table 1). Points show the SANS-derived order parameter obtained by fitting the azimuthal intensity averages with a Legendre polynomial. Error bars are the fit uncertainties. Two data points are shown for 0% 7SF PS, because this composition produced extrudates with pronounced variability in structure (Verfaillie, Li, Janssen, et al., 2024).

75:25 (w/w) 11SF:7SF led to extrudates with variable structures due to pronounced die pressure fluctuations (hence the two data points for the 0% 7SF condition in Fig. 8), whereas processing of blends richer in 7SF was more stable and resulted in layered structures, as evidenced by CLSM. Complementary MRI measurements (Fig. S5) likewise show that increasing the ratio of 7SF promotes anisotropic structure formation at the sub-mm scale.

These findings are also consistent with those reported by Fei et al. (2026), who studied commercial SPIs with varying 7S:11S globulin ratios. They reported that structural anisotropy increased as the 7S globulin content rose, reaching a maximum at a 7S:11S globulin ratio of ~ 0.64 (≈ 39% 7S globulin of total 7S+11S). Beyond this ratio, the filamentous structure formed but became more loosely arranged. Expressed in terms of the actual 7S globulin content, the 50:50 (w/w) blend in our study corresponds to ~ 30% 7S globulin (of total 7S+11S) (see secondary top axis in Fig. 8), as calculated from experimentally determined concentrations in the 7SF PS and 11SF PS (Table 1). This value falls slightly below the value reported by Fei et al. (2026) and also at the lower end of the typical 7S globulin contents reported for commercial SPCs and SPIs, which range between roughly 25% and 55% (Fei et al., 2026; Verfaillie, Li, Janssen, et al., 2024), depending on cultivar and processing history. It is important to note that in commercial SPCs and SPIs, the proteins are likely largely denatured. By contrast, in the present study, proteins were not subjected to significant heat treatment during the isolation process and therefore retained much of their native structure, which could influence the apparent optimum. Additionally, differences in analytical methods used to quantify 7S and 11S globulin content, such as SE-HPLC (Verfaillie, Li, Janssen, et al., 2024) and SDS-PAGE (Fei et al., 2026), can also introduce biases.

At first glance, these findings seem to contradict the gel results: adding 7SF at pH 7 produces weaker gels (Fig. 6) with finer and more irregular strands (Fig. 7), most notably at ≥50% 7SF. Conversely, in HME, blends with ≥50% 7SF produce more anisotropic structures. Similar to the pH-dependent trends discussed in Section 3.2, these contrasting compositional effects arise from different mechanisms that govern structure formation during gelation and HME.

In heat-set gels, network formation is governed by thermal (partial) unfolding followed by aggregation. The resulting network depends on the balance between attractive and repulsive interactions, which can be modulated either by pH or composition. In the pH series, moving away from the pI increases electrostatic repulsion, which limits aggregation and results in the formation of finer fibrillar structures with smaller mid-scale characteristic sizes. Near the pI, attractive interactions prevail, leading to larger particulate aggregates. At a constant pH of 7, the same principle applies to the compositional series. Increasing the 7S globulin content limits aggregate growth: its more negative $|\zeta|$ (Fig. 1) and hydrophilic extension regions in the α and α'-subunits enhance repulsive interactions and can terminate the growth of 11S globulin aggregates during heating (Guo et al., 2012). This results in a finer and less cohesive network, which is reflected in the observed decrease in both G' (Fig. 6) and CL (Fig. 7). In contrast, gels richer in 11S globulin form thicker and more tightly connected strands due to the high content of cysteine residues that promotes aggregation.

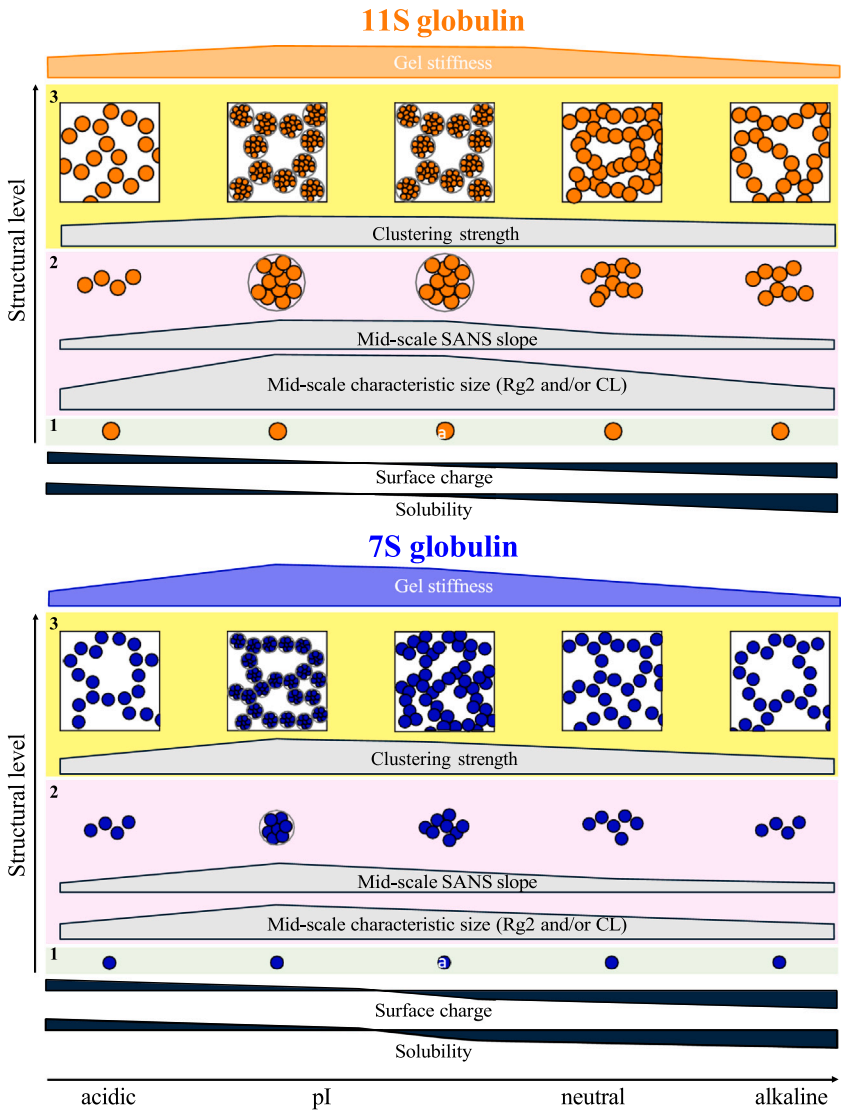


Fig. 9. Schematic summary of the effect of pH on the multiscale structural hierarchy of glycinin and β-conglycinin gels. The schematic distinguishes three structural levels: (1) moderately unfolded yet still somewhat compact protein units that persist after heating (Table S2.1) (note that this level does not resolve more subtle conformational changes within the protein molecules, e.g., dissociation state or tertiary rearrangements), (2) aggregates characterised by mid-scale characteristic size (Rg_2 and/or CL) (Fig. 4A) and SANS slope (Fig. 5), and (3) networks characterised by clustering strength (CS) (Fig. 4B). Gel stiffness (Fig. 2) is shown at the top of each panel, and surface charge (Fig. 1) at the bottom. Literature-reported trends (Jiang et al., 2010) of 7S and 11S globulins are included for reference, highlighting their correspondence with changes in aggregate morphology, connectivity and gel stiffness across pH.

Under extrusion conditions, the situation differs fundamentally. Sub-μm-scale fibrils form towards the end of the extruder section, are aligned by the flow, and are then fixed in the cooling die (Garina et al., 2024, 2026). The high protein concentration and intense shear maintain close contact between aggregates even under conditions of strong repulsion. As pH increases above the pI, the stronger charge does not suppress interactions but instead results in the formation of larger, more swollen nano-aggregates. Another factor that may contribute to the different trends between pH-shifted gels and HM extrudates (Kuijpers et al., 2025) is the variation in ionic strength. In this work, pH was adjusted using HCl and NaOH, whereas in the earlier study on the pH-shifted HME of soy proteins (Kuijpers et al., 2025), citric acid and trisodium phosphate were used. The ionic strength of these buffers is substantially different, which will influence the Debye length and thereby the range of electrostatic interactions among proteins. Under the higher ionic strength conditions of the phosphate buffer, electrostatic repulsion is more strongly screened, allowing proteins to approach more closely and aggregate into larger structures before repulsion limits further aggregation. This could explain the increasing CL with pH observed in our pH-shifted extrusion study (Kuijpers et al., 2025). Conversely, in the low ionic strength conditions of NaOH-adjusted systems, the repulsion remains long-ranged, limiting aggregation and resulting in decreased CL as pH increases. As shown in Fig. S6, structural anisotropy also differs between NaOH- and trisodium phosphate-adjusted extrudates, particularly at higher pH values, supporting the hypothesis that variation in Debye length and charge screening may also contribute to the observed structural differences. Thus, the influence of ionic strength complements the effect of shear in explaining pH-dependent aggregation behaviour. At constant pH 7, structure formation is dominated by compositional effects, with the relative proportions of 7S and 11S globulins determining structure development. Under these conditions, 7S globulin becomes particularly effective: due to its higher solubility and WHC (Fei et al., 2026; Verfaillie, Li, Janssen, et al., 2024), it promotes alignment by reducing the viscosity of the melt at the barrel exit, increasing the deformability and thus the flow-induced orientation before solidification (Li et al., 2026). The 11S globulin, on the other hand, forms strong, covalent, and relatively rigid aggregates that resist alignment under shear. As

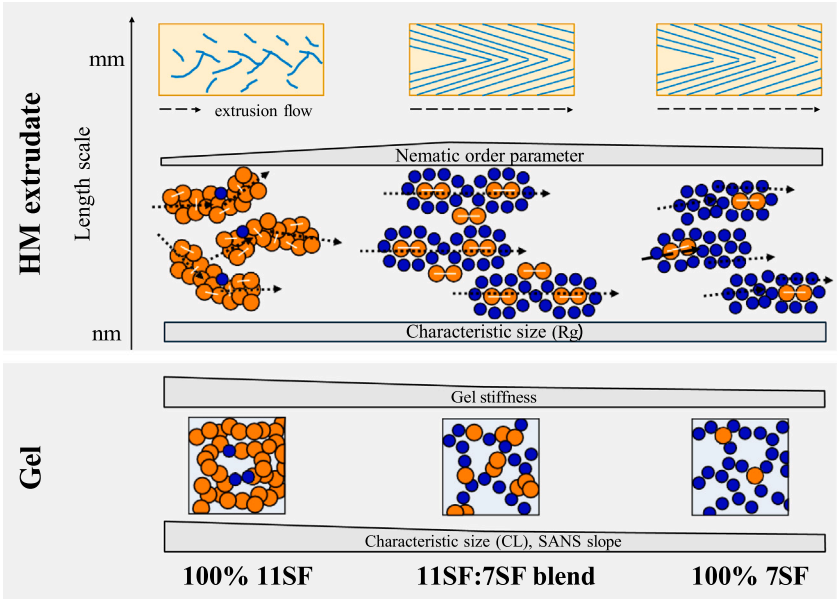


Fig. 10. Schematic summary of the effect of 11S:7S blending on gel formation and multiscale structure of HM extrudates. For gels, the effect is described by correlation length (CL) and SANS slope (Fig. 7), as well as gel stiffness (Fig. 6). For HM extrudates, the effect is described by characteristic size (Rg_2) (Table S5), nematic order parameter (Fig. 8), and sub-mm scale alignment seen in MRI (Fig. S5). The cartoons are conceptual illustrations of the experimentally observed trends and are not intended as unique reconstructions of the aggregate architecture.

a result, the 50:50 blend offers the best compromise, allowing for enhanced deformation and alignment due to 7S, while also enabling the setting of an aligned state via disulphide crosslinks during cooling, thanks to the presence of 11S. Consistent with these observations, the two-level UB fits of sector averages (parallel and perpendicular to the extrusion direction) yielded R_{g_2} that is nearly composition-independent (ca. 5.3–6.3 nm parallel; 6.2–8.1 nm perpendicular) (all fitting parameters are shown in Table S5). Furthermore, no systematic compositional trends were observed in the other fit parameters (e.g., power-law exponents). This suggests that the observed anisotropy primarily results from the alignment of existing strands rather than changes in their intrinsic size or fractal dimension.

4. Conclusions

In this work, we resolved the multiscale structural changes that underlie the effect of pH and composition on the aggregation and gelation of fractionated soy globulins, and how these changes relate to the structure formation under HME.

A schematic overview of the pH-dependent structural hierarchy in gels is given in Fig. 9. Three structural levels can be distinguished. At the first level, gels are composed of moderately unfolded yet still somewhat compact protein units that persist after heating and act as the elementary building blocks for further aggregation. The second level involves the assembly of these proteins into aggregates, with size and morphology varying with pH. At pH ~ pI, electrostatic repulsion is minimal and attractive interactions dominate, leading to extensive, random aggregation. As a result, particulate aggregation predominates and large, spherical aggregates are formed. This regime is indicated by the largest mid-scale characteristic sizes and local SANS slopes of about -3. Moving away from the pI, the net charge on the proteins increases, suppressing random particulate aggregation and favouring more ordered aggregation pathways. Correspondingly, mid-scale characteristic sizes decrease and the slopes fall between −1.3 and −1.7, reflecting the presence of smaller, more linear fibrillar aggregates. At pH ≫ or ≪ pI, electrostatic repulsion is strongest; aggregation is limited to thin, weakly clustered fibrils, as evidenced by further reduced and SANS slopes approaching -1, consistent with the formation of thin, loosely connected fibrils. Across all pH conditions, 11S soy globulins tend to form larger aggregates than 7S globulins, reflecting protein-specific properties. Above the pI, the pI, the lower net charge and higher hydrophobic exposure and cysteine content of 11S globulin favours aggregation and stabilisation of larger aggregates over a broader pH range. In contrast, 7S globulin, with higher net charge and lower crosslinking capacity, shows more pronounced pH-driven changes in aggegation, forming smaller and more weakly associated fibrillar structures at pH ≫ pI. At the third level, the connectivity of aggregates is captured by the clustering strength (CS). In general, CS is highest near the pI and decreases when moving away from it. The 7S soy globulin exhibits more pronounced changes in CS across the pH range, whereas the 11S globulin maintains elevated CS over a broader pH window. Near the pI, the 7S globulin has higher CS than 11S globulin because its smaller aggregates allow a greater number of contacts per unit volume. Moving away from the pI, 11S globulins form thicker and more tightly connected strands, resulting in a more cohesive network and a higher CS than 7S globulins. These pH-dependent trends in aggregate morphology and their connectivity are consistent with solubility trends reported in the literature: protein solubility is lowest near the pI, where extensive aggregation and strong network connectivity are observed, and increases at more acidic or alkaline pH, where aggregate connectivity decreases. Taken together, these three structural levels provide a mechanistic framework for understanding the observed rheological behaviour: 7S-globulin-enriched gels are stiffer near the pI, whereas 11S-globulin-enriched gels maintain higher stiffness away from it. Importantly, the same pH-dependent aggregation regimes identified here for static heat-set gels mirror those previously observed during pH-shifted HME of SPC, indicating that pH-induced changes in protein-protein interactions govern structure formation in both systems, despite the presence of process-specific differences. We note that the present conclusions are drawn from enriched globulin fractions, and future work using more highly purified 7S and 11S globulins would be valuable to further isolate the contributions of each component.

A schematic overview of the effect of 11S:7S globulin blending on gel formation and multiscale structure of HM extrudates is given in Fig. 10. The addition of 7S globulins weakens the gel network: the characteristic size (CL) and SANS slope decrease sharply reflecting a transition from thick, tightly connected 11S-globulin-rich strands to finer and

more weakly connected 7S-globulin-rich structures, and a corresponding drop in gel strength. In extrudates, however, the same addition of 7S soy globulins has the opposite effect, promoting the development of anisotropy on multiple length scales. Here, the characteristic size (Rg) is insensitive to composition, and the nematic order parameter captures the blending effect: 11S-globulin-rich systems form rigid aggregates that resist alignment, 7S-globulin-rich systems deform and align more readily, and blends strike the balance by combining deformability (7S globulin) with the ability of 11S globulins to set the aligned state via covalent crosslinks. Together, these results demonstrate that while 7S globulin addition weakens gels, it has a positive effect on anisotropy development in HM extrudates, highlighting the complementary roles of the two globulins. Optimal anisotropic structure formation during HME occurred at 30% 7S globulin (of total 7S+11S), a slightly lower optimum than what has been reported for SPIs and SPCs. Given that the proteins used in the present study remained largely native, further research should investigate whether this discrepancy arises from the partially denatured state of proteins in commercial SPIs/SPCs or from differences in analytical methods used to quantify 7S and 11S globulin contents. Extending this work to include 11S and 7S globulins from other legumes would also be valuable, as their aggregation and gelation behaviours differ markedly from those of soy and the underlying causes of these differences are not yet fully understood.

CRediT authorship contribution statement

Ekaterina D. Garina: Writing – original draft, Visualization, Methodology, Investigation, Formal analysis, Data curation, Conceptualization. **Sam A. Kuijpers:** Data curation. **Martijn I. Gobes:** Data curation. **Gregory N. Smith:** Writing – review & editing, Software, Data curation. **Michael Sztucki:** Writing – review & editing, Software, Data curation. **Arno G.B. Wouters:** Writing – review & editing, Resources, Investigation, Conceptualization. **John P.M. van Duynhoven:** Writing – review & editing, Supervision, Resources, Funding acquisition, Conceptualization. **Wim G. Bouwman:** Writing – review & editing, Supervision, Resources, Funding acquisition, Conceptualization.

Declaration of competing interest

The authors declare the following financial interests/personal relationships which may be considered as potential competing interests: John P.M. van Duynhoven is employed by a company that manufactured and marketed plant-based meat alternatives. The other authors declare that they have no known competing financial interests or personal relationships that could have appeared to influence the work reported in this paper.

Acknowledgements

This work is part of the project “Measurement and Modelling of Multiscale Processed Protein Products (MP3)” (with project number 18744) of the research programme OPT TTW, which is financed by the Dutch Research Council as well as by contributions from consortium partners Unilever, Cargill, dsm-firmenich, FrieslandCampina and Wageningen Food and Biobased Research. We gratefully acknowledge the Science and Technology Facilities Council (STFC) for access to neutron beamtime at ISIS through RB 2569002. We also acknowledge the European Synchrotron Radiation Facility (ESRF) for the provision of synchrotron radiation facilities. This project was further supported by the uNMR-NL Grid: A distributed, state-of-the-art Magnetic Resonance facility for the Netherlands (NWO grant 184.035.002). This work benefited from the use of the SasView application, originally developed under NSF Award DMR-0520547. SasView also contains code developed with funding from the EU Horizon 2020 programme under the SINE2020 project Grant No. 654000. We thank Remco Koppert for helping with the rheology measurements, Peter De Groot - for helping with the zeta potential measurements, Jiashu Li - for performing SE-HPLC analysis, Niels de Roo and Courtney Leigh - for lipid and fibre analyses.

Appendix A. Supplementary data

Supplementary material related to this article can be found online at https://doi.org/10.1016/j.foodhyd.2026.112567.

Data availability

Data will be made available on request.

References

Arnold, O., Bilheux, J. C., Borreguero, J. M., Buts, A., Campbell, S. I., Chapon, L., Doucet, M., Draper, N., Ferraz Leal, R., Gigg, M. A., Lynch, V. E., Markvardsen, A., Mikkelson, D. J., Mikkelson, R. L., Miller, R., Palmen, K., Parker, P., Passos, G., Perring, T. G., ... Zikovsky, J. (2014). Mantid - data analysis and visualization package for neutron scattering and μ SR experiments. *Nuclear Instruments and Methods in Physics Research, Section A: Accelerators, Spectrometers, Detectors and Associated Equipment*, *764*, 156–166. http://dx.doi.org/10.1016/j.nima.2014.07.029.

Badley, R. A., Atkinson, D., Hauser, H., Oldani, D., Green, J. P., & Stubbs, J. M. (1975). The structure, physical and chemical properties of the soy bean protein glycinin. *Biochimica Et Biophysica Acta (BBA) - Protein Structure*, *412*(2), 214–228. http://dx.doi.org/10.1016/0005-2795(75)90036-7.

Beaucage, G. (1995). Approximations leading to a unified exponential/power-law approach to small-angle scattering. *Journal of Applied Crystallography*, *28*(6), 717–728. http://dx.doi.org/10.1107/S0021889895005292.

Beaucage, G. (1996). Small-angle scattering from polymeric mass fractals of arbitrary mass-fractal dimension. *Journal of Applied Crystallography*, *29*(2), 134–146. http://dx.doi.org/10.1107/S0021889895011605.

Chinchalikar, A. J., Aswal, V. K., Kohlbrecher, J., & Wagh, A. G. (2013). Small-angle neutron scattering study of structure and interaction during salt-induced liquid-liquid phase transition in protein solutions. *Physical Review E - Statistical, Nonlinear, and Soft Matter Physics*, *87*(6), Article 062708. http://dx.doi.org/10.1103/PhysRevE.87.062708.

Damodaran, S., & Kinsella, J. E. (1982). Effect of conglycinin on the thermal aggregation of glycinin. *Journal of Agricultural and Food Chemistry*, *30*(5), 812–817. http://dx.doi.org/10.1021/jf00113a003.

Doi, E. (1993). Gels and gelling of globular proteins. *Trends in Food Science & Technology*, *4*(1), 1–5. http://dx.doi.org/10.1016/S0924-2244(05)80003-2.

Doi, E., & Kitabatake, N. (1989). Structure of glycinin and ovalbumin gels. *Food Hydrocolloids*, *3*(4), 327–337. http://dx.doi.org/10.1016/S0268-005X(89)80043-8.

Doucet, M., Cho, J. H., Alina, G., Attala, Z., Bakker, J., Bouwman, W., Bourne, R., Butler, P., Cadwallader-Jones, I., Campbell, K., Cooper-Benun, T., Durniak, C., Forster, L., Gilbert, P., Gonzalez, M., Heenan, R., Jackson, A., King, S., Kienzle, P., ... Wolf, C. (2025). SasView version 6.1.1. http://dx.doi.org/10.5281/zenodo.17237394.

Fei, C., Li, L., Zhao, R., Wang, X., Fan, B., Liu, L., Wang, F., & Huang, Y. (2026). Texture and structure of high-moisture extrudates produced from soybean protein isolates with different 7S/11S globulin ratios. *Food Hydrocolloids*, *171*, Article 111771. http://dx.doi.org/10.1016/j.foodhyd.2025.111771.

Gao, K., Rao, J., & Chen, B. (2024). Plant protein solubility: A challenge or insurmountable obstacle. *Advances in Colloid and Interface Science*, *324*, Article 103074. http://dx.doi.org/10.1016/j.cis.2023.103074.

Garina, E. D., den Adel, R., van Duynhoven, J. P., Smith, G. N., Dalgliesh, R. M., Sztucki, M., & Bouwman, W. G. (2024). SANS and SAXS: A Love story to unravel structural evolution of soy proteins and polysaccharide fibres during high moisture extrusion for meat alternatives. *Food Hydrocolloids*, *155*, Article 110121. http://dx.doi.org/10.1016/J.FOODHYD.2024.110121.

Garina, E. D., Kuijpers, S. A., Gobes, M. I., Sein, A., den Adel, R., Smith, G. N., Sztucki, M., Hohlbein, J., Terenzi, C., van Duynhoven, J. P., & Bouwman, W. G. (2026). Mapping anisotropic structure formation of soy protein during high-moisture extrusion. *Food Hydrocolloids*, *172*, Article 112037. http://dx.doi.org/10.1016/j.foodhyd.2025.112037.

Guan, T., Sägesser, C., Villiger, R., Zychowski, L., Kohlbrecher, J., Dumpler, J., Mathys, A., Rühs, P., Fischer, P., & Matsarskaia, O. (2024). In situ studies of plant-based meat analog texturization. *Food Hydrocolloids*, *155*, Article 110215. http://dx.doi.org/10.1016/j.foodhyd.2024.110215.

Guo, J., Yang, X. Q., He, X. T., Wu, N. N., Wang, J. M., Gu, W., & Zhang, Y. Y. (2012). Limited aggregation behavior of β-conglycinin and its terminating effect on glycinin aggregation during heating at pH 7.0. *Journal of Agricultural and Food Chemistry*, *60*(14), 3782–3791. http://dx.doi.org/10.1021/jf300409y.

Hammouda, B., Ho, D. L., & Kline, S. (2004). Insight into clustering in poly(ethylene oxide) solutions. *Macromolecules*, *37*(18), 6932–6937. http://dx.doi.org/10.1021/ma049623d.

Hatzakis, E., Agiomyrgianaki, A., Kostidis, S., & Dais, P. (2011). High-resolution NMR spectroscopy: An alternative fast tool for qualitative and quantitative analysis of diacylglycerol (DAG) oil. *Journal of the American Oil Chemists' Society*, *88*(11), 1695–1708. http://dx.doi.org/10.1007/s11746-011-1848-2.

Hermansson, A. M. (1979). Aggregation and denaturation involved in gel formation. *ACS Symposium Series*, (92), 81–103. http://dx.doi.org/10.1021/bk-1979-0092.ch005.

Hermansson, A.-M.-M. (1985). Structure of soya glycinin and conglycinin gels. *Journal of the Science of Food and Agriculture*, *36*(9), 822–832. http://dx.doi.org/10.1002/jsfa.2740360911.

ISIS Larmor 2023. https://www.isis.stfc.ac.uk/Pages/Larmor.aspx. (Accessed 21 July 2023).

Jiang, J., Xiong, Y. L., & Chen, J. (2010). pH shifting alters solubility characteristics and thermal stability of soy protein isolate and its globulin fractions in different pH, salt concentration, and temperature conditions. *Journal of Agricultural and Food Chemistry*, *58*(13), 8035–8042. http://dx.doi.org/10.1021/jf101045b.

Khalesi, M., Glenn-Davi, K., Mohammadi, N., & FitzGerald, R. J. (2024). Key factors influencing gelation in plant vs. Animal proteins: A comparative mini-review. *Gels*, *10*(9), 575. http://dx.doi.org/10.3390/gels10090575.

Kinsella, J. E. (1979). Functional properties of soy proteins. *Journal of the American Oil Chemists' Society*, *56*(3), 242–258. http://dx.doi.org/10.1007/BF02671468.

Koshiyama, I. (1968). Chromatographic and sedimentation behavior of a purified 7S protein in soybean globulins. *Cereal Chemistry*, *45*, 405–412.

Koshiyama, I. (1972). Purification and physico-chemical properties of 11S globulin in soybean seeds. *International Journal of Peptide and Protein Research*, *4*(3), 167–176. http://dx.doi.org/10.1111/J.1399-3011.1972.TB03416.X.

Kuijpers, S. A., Garina, E. D., Gobes, M. I., Adel, R. d., Smith, G. N., Sztucki, M., Hohlbein, J., Bouwman, W. G., van Duynhoven, J. P., & Terenzi, C. (2025). Impact of pH-shifting on multiscale structural anisotropy of high-moisture extrudates of soy proteins. *Food Hydrocolloids*, *168*, Article 111456. http://dx.doi.org/10.1016/j.foodhyd.2025.111456.

Lakemond, C. M., de Jongh, H. H., Paques, M., van Vliet, T., Gruppen, H., & Voragen, A. G. (2003). Gelation of soy glycinin; influence of pH and ionic strength on network structure in relation to protein conformation. *Food Hydrocolloids*, *17*(3), 365–377. http://dx.doi.org/10.1016/S0268-005X(02)00100-5.

Li, J., Janssen, F., Vallaey, A., Verfaillie, D., Brijs, K., Delcour, J. A., van der Goot, A. J., Van Royen, G., & Wouters, A. G. (2026). Understanding the effect of pH on structure formation in high moisture extrudates produced from soy protein-dietary fiber blends. *Food Hydrocolloids*, *170*, Article 111710. http://dx.doi.org/10.1016/j.foodhyd.2025.111710.

Merkx, D. W. H., Westphal, Y., van Velzen, E. J., Thakoer, K. V., de Roo, N., & van Duynhoven, J. P. (2018). Quantification of food polysaccharide mixtures by 1H NMR. *Carbohydrate Polymers*, *179*, 379–385. http://dx.doi.org/10.1016/j.carbpol.2017.09.074.

Nagano, T., Hirotsuka, M., Mori, H., Kohyama, K., & Nishinari, K. (1992). Dynamic viscoelastic study on the gelation of 7S globulin from soybeans. *Journal of Agricultural and Food Chemistry*, *40*(6), 941–944. http://dx.doi.org/10.1021/jf00018a004.

Nagano, T., Mori, H., & Nishinari, K. (1994). Effect of heating and cooling on the gelation kinetics of 7S globulin from soybeans. *Journal of Agricultural and Food Chemistry*, *42*(7), 1415–1419. http://dx.doi.org/10.1021/jf00043a005.

Narayanan, T., Sztucki, M., Zinn, T., Kieffer, J., Homs-Puron, A., Gorini, J., Van Vaerenbergh, P., & Boesecke, P. (2022). Performance of the time-resolved ultra-small-angle X-ray scattering beamline with the extremely brilliant source. *Journal of Applied Crystallography*, *55*(1), 98–111. http://dx.doi.org/10.1107/S1600576721012693.

Renkema, J. M. (2004). Relations between rheological properties and network structure of soy protein gels. *Food Hydrocolloids*, *18*(1), 39–47. http://dx.doi.org/10.1016/S0268-005X(03)00040-7.

Renkema, J. M., Gruppen, H., & Van Vliet, T. (2002). Influence of pH and ionic strength on heat-induced formation and rheological properties of soy protein gels in relation to denaturation and their protein compositions. *Journal of Agricultural and Food Chemistry*, *50*(21), 6064–6071. http://dx.doi.org/10.1021/jf020061b.

Renkema, J. M., Knabben, J. H., & Van Vliet, T. (2001). Gel formation by β-conglycinin and glycinin and their mixtures. *Food Hydrocolloids*, *15*(4–6), 407–414. http://dx.doi.org/10.1016/S0268-005X(01)00051-0.

Renkema, J. M., Lakemond, C. M., de Jongh, H. H., Gruppen, H., & Van Vliet, T. (2000). The effect of pH on heat denaturation and gel forming properties of soy proteins. *Journal of Biotechnology*, *79*(3), 223–230. http://dx.doi.org/10.1016/S0168-1656(00)00239-X.

Staswick, P. E., Hermodson, M. A., & Nielsen, N. C. (1984). Identification of the cystines which link the acidic and basic components of the glycinin subunits. *Journal of Biological Chemistry*, *259*(21), 13431–13435. http://dx.doi.org/10.1016/S0021-9258(18)90712-X.

Stradner, A., Cardinaux, F., & Schurtenberger, P. (2006). A small-angle scattering study on equilibrium clusters in lysozyme solutions. *Journal of Physical Chemistry B*, *110*(42), 21222–21231. http://dx.doi.org/10.1021/jp0639804.

Svergun, D., Barberato, C., & Koch, M. H. (1995). CRYSOL - A program to evaluate X-ray solution scattering of biological macromolecules from atomic coordinates. *Journal of Applied Crystallography*, *28*(6), 768–773. http://dx.doi.org/10.1107/S0021889895007047.

Sztucki, M. (2021). SAXSutilities: a graphical user interface for processing and analysis of small-angle X-ray scattering data (1.024). http://dx.doi.org/10.5281/zenodo.5825707.

Thanh, V. H., & Shibasaki, K. (1977). Beta-conglycinin from soybean proteins. Isolation and immunological and physicochemical properties of the monomeric forms. *Biochimica Et Biophysica Acta (BBA) - Protein Structure*, *490*(2), 370–384. http://dx.doi.org/10.1016/0005-2795(77)90012-5.

Tiong, A. Y., Crawford, S., de Campo, L., Ryukhtin, V., Garvey, C. J., Batchelor, W., & van 't Hag, L. (2025). Legume protein gelation: The mechanism behind the formation of homogeneous and fractal gels. *Food Hydrocolloids*, *159*, Article 110639. http://dx.doi.org/10.1016/j.foodhyd.2024.110639.

Utsumi, S., & Kinsella, J. E. (1985). Forces involved in soy protein gelation: Effects of various reagents on the formation, hardness and solubility of heat-induced gels made from 7s, 11s, and soy isolate. *Journal of Food Science*, *50*(5), 1278–1282. http://dx.doi.org/10.1111/j.1365-2621.1985.tb10461.x.

Verfaillie, D., Li, J., Janssen, F., Blontrock, E., Van Royen, G., & Wouters, A. G. (2024). Structure formation in high moisture extrudates produced from soy protein fractions varying in 7S/11S globulin ratio. *International Journal of Biological Macromolecules*, *283*, Article 137369. http://dx.doi.org/10.1016/j.ijbiomac.2024.137369.

Verfaillie, D., Li, J., Van Droogenbroeck, B., Pannecoucque, J., Tavernier, G., Van Royen, G., & Wouters, A. G. (2024). Genetic and environmental variation in protein composition of belgian soy determined with a novel size-exclusion chromatography method. *Journal of Food Composition and Analysis*, *130*, Article 106187. http://dx.doi.org/10.1016/j.jfca.2024.106187.

Weijers, M., De Hoog, E. H., Cohen Stuart, M. A., Visschers, R. W., & Barneveld, P. A. (2005). Heat-induced formation of ordered structures of ovalbumin at low ionic strength studied by small angle X-ray scattering. *Colloids and Surfaces A: Physicochemical and Engineering Aspects*, *270–271*(1–3), 301–308. http://dx.doi.org/10.1016/j.colsurfa.2005.07.001.

Wignall, G. D., & Bates, F. S. (1987). Absolute calibration of small-angle neutron scattering data. *Journal of Applied Crystallography*, *20*(1), 28–40. http://dx.doi.org/10.1107/S0021889887087181.

Wu, S., Murphy, P. A., Johnson, L. A., Fratzke, A. R., & Reuber, M. A. (1999). Pilot-plant fractionation of soybean glycinin and β-conglycinin. *Journal of the American Oil Chemists' Society*, *76*(3), 285–293. http://dx.doi.org/10.1007/S11746-999-0233-X.

Xiao, J., Shi, C., Zhang, L., Li, Y., Qi, J., Wang, Y., & Huang, Q. (2016). Multilevel structural responses of β -conglycinin and glycinin under acidic or alkaline heat treatment. *Food Research International*, *89*, 540–548. http://dx.doi.org/10.1016/j.foodres.2016.09.006.

Yang, Z., Li, D., Chen, L., Zhang, W., Jiang, L., Huang, Z., & Tian, T. (2024). Structural characteristics, techno-functionalities, innovation applications and future prospects of soybean β-conglycinin/glycinin: a comprehensive review. *Critical Reviews in Food Science and Nutrition*, http://dx.doi.org/10.1080/10408398.2024.2440601.

Yuan, D. B., Yang, X. Q., Tang, C. H., Zheng, Z. X., Wei-Min, Ahmad, I., & Yin, S. W. (2009). Physicochemical and functional properties of acidic and basic polypeptides of soy glycinin. *Food Research International*, *42*(5–6), 700–706. http://dx.doi.org/10.1016/j.foodres.2009.02.005.